Journal of Luminescence 234 (2021) 117955

Contents lists available at ScienceDirect

Journal of Luminescence

journal homepage: http://www.elsevier.com/locate/jlumin

# Sub-nanosecond, high peak power Yb:YAG/$Cr^{4+}$:YAG/$YVO_4$ passively Q-switched Raman micro-laser operating at 1134 nm

Xiao-Lei Wang [a,b], Xiao-Jie Wang [a], Jun Dong [a,*]

[a] Laboratory of Laser and Applied Photonics (LLAP), Department of Electronic Engineering, Xiamen University, Xiamen, 361005, China
[b] CAS Key Laboratory of Separation Sciences for Analytical Chemistry, Dalian Institute of Chemical Physics, Chinese Academy of Sciences, Dalian, 116023, China

ARTICLE INFO

*Keywords:*
Yb:YAG
$YVO_4$
micro-lasers
Passively Q-switched
Raman lasers

ABSTRACT

We demonstrate a sub-nanosecond, high peak power Yb:YAG/$Cr^{4+}$:YAG/$YVO_4$ passively Q-switched Raman micro-laser (PQSRML) operating at 1134 nm. The effect of transmission of the output coupler ($T_{OC}$) and $Cr^{4+}$:YAG initial transmission ($T_0$) on the Raman laser performance have been investigated. Stable Raman laser pulse trains have been observed for Yb:YAG/$Cr^{4+}$:YAG/$YVO_4$ PQSRMLs with different combinations of output couplers and $Cr^{4+}$:YAG crystals. Maximum average output power of Raman laser was 142.8 mW with $T_{OC}$ = 11% output coupler and $T_0$ = 90% $Cr^{4+}$:YAG. Enhanced Stokes pulse performance of 24.1 μJ, 45.1 kW, 535 ps was achieved with $T_{OC}$ = 16% and $T_0$ = 85% $Cr^{4+}$:YAG. A modified Raman laser rate equation model is established and the theoretically calculated results are in fairly good agreement with experimental results.

## 1. Introduction

Laser-diode (LD) end-pumped $Cr^{4+}$:YAG passively Q-switched micro-lasers (PQSMLs) can produce sub-nanosecond or even picosecond pulses maintaining modest pulse energy and high peak power. PQSMLs possess merits of high compactness, good stability, low cost and easy alignment. However, emitting wavelengths of conventional PQSMLs are limited by the spontaneous fluorescence spectra of rare-earth ions. PQSMLs operating around 1.1 μm are still difficult to fabricate due to short of appropriate laser materials with high gain and suitable saturable absorbers (SAs). Lasers oscillating around 1120–1150 nm can be used to generate yellow-green lasers by frequency doubling [1,2], which have growing demand for many biomedicine applications such as cytology, ophthalmology, dermatology and laser-based confocal microscopes. Especially, 0.56 μm yellow-green laser radiation has important applications in flow cytometers because of its excellent excitation efficiency of phycoerythrin (PE) and red fluorescent proteins (DsRed and dTomato) [3–6]. The frequency doubling of 1123 nm Nd:YAG laser has been identified as a common method for obtaining 561 nm yellow-green laser radiation. However, the low strength of transition (R1→Y6) of Nd:YAG crystal for generating 1123 nm leads to the lasers require extra frequency selectors such as etalon, birefringent filter and volume Bragg gratings or specially designed coatings, which makes the lasers complicated and high cost. Therefore, more efforts should be made for developing miniature, high peak power pulsed laser sources around 1120–1150 nm. Stimulated Raman scattering (SRS) is an alternative method to generate special laser radiations, which are difficultly achieved from the straightforward lasing of common rare-earth ions doped laser gain media, for instance at 1120–1150 nm. Combining the SRS process with LD pumped PQSML technique is a promising approach to achieve sub-nanosecond laser pulses and meanwhile expand the spectral region of conventional PQSMLs.

Yttrium vanadate ($YVO_4$) crystals have been recognized as effective Raman media because of excellent optical and mechanical properties such as large damage threshold, high Raman gain and a wide spectral transparent range [7]. In 2018, simultaneous dual-wavelength Raman laser emitting at 1164.4 nm and 1174.7 nm with sub-nanosecond pulse performance directly pumped by 880 nm LD has been demonstrated from the Nd:$GdVO_4$/$Cr^{4+}$:YAG/$YVO_4$ PQSRML [8]. Ytterbium (Yb) ions doped laser materials possess several advantages over $Nd^{3+}$ ions doped laser gain media, such as simple energy structure, low quantum defect, wide absorption spectrum, long fluorescence lifetime and permitting high doping concentration [9]. Therefore, $Yb^{3+}$ doped laser materials are desirable for developing sub-nanosecond PQSRMLs. Sub-nanosecond PQSMLs utilizing Yb:YAG [10,11] and Yb:$KLu(WO_4)_2$ [12] crystals as laser gain media and $Cr^{4+}$:YAG crystals as SAs operating around 1 μm have been investigated. $Cr^{4+}$:YAG passively Q-switched self-Raman lasers based on $Yb^{3+}$:$KGd(WO_4)_2$ [13,14], $Yb^{3+}$:$KY(WO_4)_2$

* Corresponding author.
*E-mail address:* jdong@xmu.edu.cn (J. Dong).

https://doi.org/10.1016/j.jlumin.2021.117955
Received 5 September 2020; Received in revised form 20 December 2020; Accepted 2 February 2021
Available online 4 February 2021

[15], Yb:KLu$(WO_4)_2$ [16–18] and $Yb^{3+}$:$YVO_4$ [19] crystals producing first-order Stokes laser around 1120–1150 nm have been demonstrated. However, the shortcomings of self-Raman lasers are severe thermal loading. The utilization of discrete laser gain medium and Raman medium is an effective strategy for good thermal management to avoid severe thermal loading. In 2018, a multi-wavelength, sub-nanosecond Yb:YAG/$Cr^{4+}$:YAG/$YVO_4$ PQSRML emitting Raman laser at 1–1.26 μm with a pulse duration of 440 ps and peak power of 9.2 kW has been obtained [20].

For most conventional intracavity Raman lasers, in order to acquire high intracavity power density, output couplers are always high-reflection (HR) coated for fundamental laser wavelengths and meanwhile suitable partial transmission (PR) for desired Raman laser lines. However, it makes huge challenges for the coating technique. The damage threshold of the complicated coating film may be reduced. Consequently, the deliberately designed coating film of OCs makes the laser system high cost and unsuitable for high peak power operation. It is valuable to find a straightforward and convenient method for developing low-cost PQSRMLs with stable operation under high peak power level.

In this paper, sub-nanosecond Raman laser pulses at 1134 nm have been obtained from a LD pumped PQSRML using Yb:YAG as laser crystal and *c*-cut $YVO_4$ as Raman crystal. The OCs used in the experiment are originally designed for 1 μm Yb:YAG laser without specific coating for particular Raman laser wavelength. The dependence of the Raman laser performance on the transmission of output couplers and initial transmission of $Cr^{4+}$:YAG have been investigated.

## 2. Experimental setup

The experimental configuration of LD pumped Yb:YAG/$Cr^{4+}$:YAG/$YVO_4$ PQSRML for generating 1134 nm Raman laser is shown in Fig. 1 (a). The energy level diagrams for a typical quasi-three-level Yb:YAG crystal is shown in Fig. 1(b). A continuous-wave (CW), fiber-coupled LD arrays emitting at 940 nm with a fiber core size of 200 μm and numerical aperture (N.A.) of 0.22 was employed as the pump source. The optical coupling system was a combination of two aspheric lenses with 8 mm focal length. A 1.2-mm-thick, 10 at.% doped Yb:YAG crystal was used as the laser gain medium. The rear surface of the Yb:YAG crystal was coated with anti-reflection (AR) at 940 nm and high-reflected at 1030–1100 nm (R > 99.8%) to serve as the rear cavity mirror of the micro-laser resonator. A 3-mm thick, *c*-cut $YVO_4$ crystal was used as the Raman active medium. Two different $Cr^{4+}$:YAG samples with $T_0 = 90\%$ and 85% were used as the saturable absorbers. The corresponding thicknesses were 0.5 mm and 0.8 mm, respectively. Several 2-mm-thick commercial BK7 plane mirrors with different $T_{OC}$s from 2% to 16% at 1030 nm originally designed for 1 μm Yb:YAG laser were employed as OCs. The transmissions of OCs for fundamental laser at 1030 nm were measured to be 2%, 6%, 11%, 16%. For Raman laser at 1134 nm, the transmissions of OCs were 3%, 7%, 13%, 18%, which differed by approximately 1%–3% from that of fundamental laser. All optical cavity elements were mounted in mechanical contact as close as possible with each other by a pair of copper plates with 3 mm diameter central holes. The copper holders were also served as the heat sink to mitigate the heat accumulation. The experiments were carried out at room temperature and no active cooler were applied. The overall geometrical cavity length is shortened to be only 4.7 mm or 5 mm depending on the length of $Cr^{4+}$:YAG crystals. The average output power was measured by a Thorlabs PM200 power meter in the experiment. An Anritsu optical spectral analyzer (MS9740A) was employed to record the emitting laser spectra. A digital oscilloscope (6 GHz bandwidth, TDS6604, Tektronix Inc.) and a 5 GHz InGaAs photo-diode were used to record and analysis the laser pulse characteristics.

## 3. Experimental results

### 3.1. Effects of $T_{OC}$ on laser performance of Yb:YAG/$Cr^{4+}$:YAG/$YVO_4$ PQSRML

The effect of $T_{OC}$ on the performance of the Yb:YAG/$Cr^{4+}$:YAG/$YVO_4$ PQSRML was studied when the $T_0$ of $Cr^{4+}$:YAG crystal was set to 90%. For the Yb:YAG/$Cr^{4+}$:YAG/$YVO_4$ PQSRML with $T_0 = 90\%$ SA, the evolution of the typical emission spectra with $T_{OC}$s at $P_{in} = 3.9$ W is shown in Fig. 2(a)–(d). An enlarged emission spectrum with fine spectral information for $T_{OC} = 6\%$ is shown in Fig. 2(e). The emission spectra contain both Raman laser and residual fundamental laser. The 1134 nm Raman laser is converted from 1030 nm fundamental laser via the strongest Raman frequency shift of 890 $cm^{-1}$ for the *c*-cut $YVO_4$ crystal. The spectral intensity ratios of the Raman laser to the fundamental laser increased with the decrease of $T_{OC}$. The simultaneous emitting of fundamental laser and Raman laser with high peak power is favorable for the generation of several visible lines such as 515 nm and 567 nm or even ultraviolet radiation wavelengths by SHG (second harmonic generation) or SFG (sum-frequency generation).

The multi-longitudinal mode oscillation was dominant in the Yb:YAG/$Cr^{4+}$:YAG/$YVO_4$ PQSRML with different $T_{OC}$s due to the wide spontaneous emission spectra of Yb:YAG crystal. For $Cr^{4+}$:YAG passively Q-switched lasers, the laser pulses growth process also provides a natural selection mechanism of oscillating longitudinal modes [21]. As $Cr^{4+}$:YAG is a "slow" saturable absorber, the growth of laser pulse intensity is very slow and a large number of passes is required for the laser pulses arise from the noise level to its peak value. This time is long enough for the effective longitudinal modes selection. Generally, the emitting spectrum in the case of passively Q-switched operation is

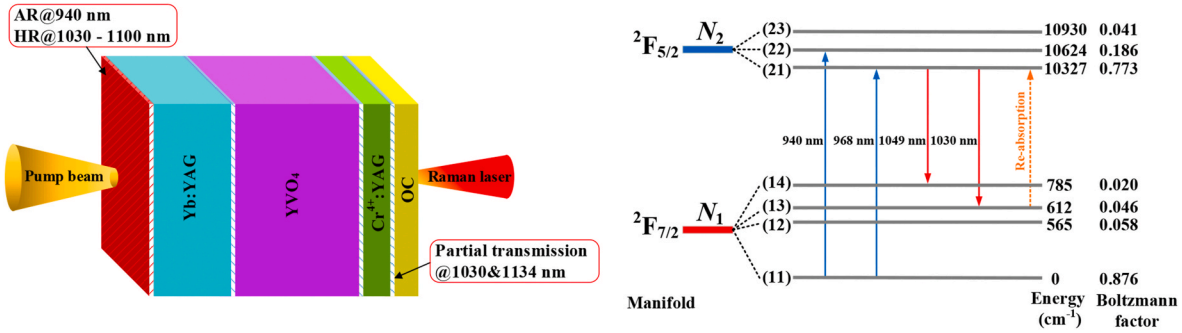


**Fig. 1.** (a) Schematic diagram of Yb:YAG/$Cr^{4+}$:YAG/$YVO_4$ PQSRML. (b) Energy level diagrams of $Yb^{3+}$ ion. The calculated Boltzmann occupation factors at room temperature (300 K) are also shown.

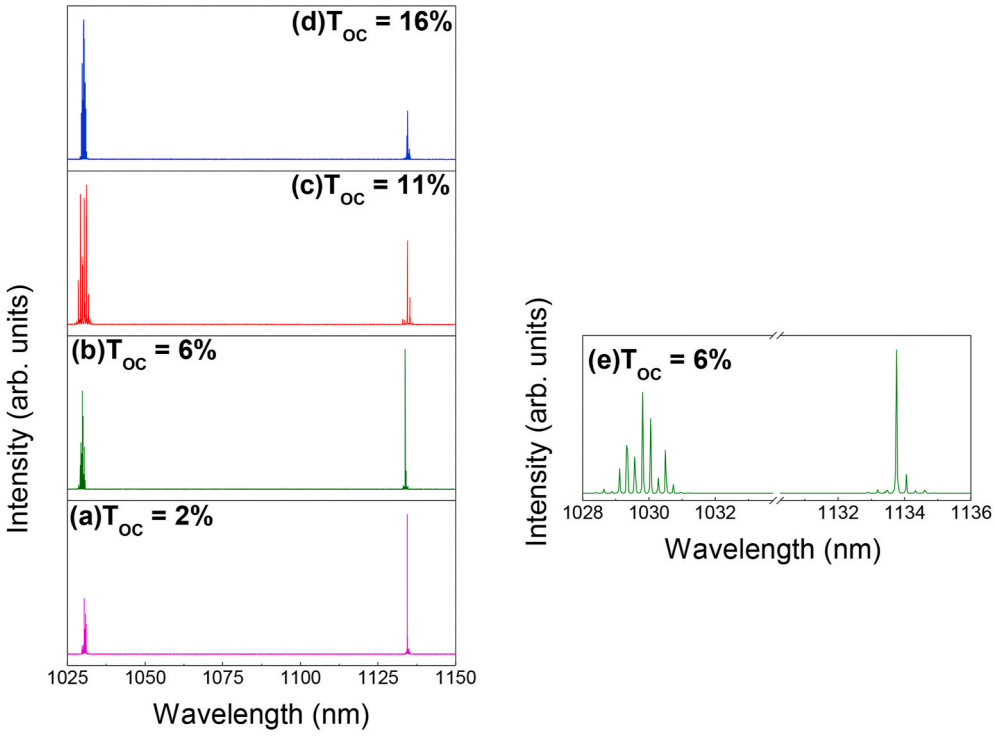


**Fig. 2.** (a)–(d) Typical emission spectra of Yb:YAG/$Cr^{4+}$:YAG/$YVO_4$ PQSRML for various $T_{OC}$s at $P_{in}$ = 3.9 W. (e) Enlarged emission spectrum with fine spectral information for $T_{OC}$ = 6%.

usually narrower compared with CW performance, indicating that single longitudinal mode output can be achieved with $Cr^{4+}$:YAG saturable absorber under some certain circumstances [22–25]. The longitudinal modes separations for 1030 nm fundamental laser and 1134 nm Raman laser were measured to be approximately 0.23 and 0.29 nm, respectively, as shown in Fig. 2(e). The longitudinal modes separations of fundamental laser and Raman laser are about 3.8 and 3.9 times of the free spectral range (FSR) of the Yb:YAG/$Cr^{4+}$:YAG/$YVO_4$ PQSRML, respectively, which is determined by $\Delta\lambda = \lambda^2/2L_C$ [26] where $L_C$ is the optical length of the laser resonator and $\lambda$ is the wavelength of the fundamental laser or Raman laser. The wide longitudinal mode spacing for both fundamental and Raman laser is mainly due to the mode selection property of the tilted intracavity etalon by the 1.2-mm-thick Yb:YAG crystal. The number of Raman laser longitudinal modes is obvious less than that of fundamental laser indicating that a cleaning effect of multi-longitudinal mode for fundamental laser can be achieved by the SRS process.

First, the dependence of the Raman laser average output power of Yb:YAG/$Cr^{4+}$:YAG/$YVO_4$ PQSRML on $T_{OC}$s was investigated with $T_0$ = 90% $Cr^{4+}$:YAG crystal as SA, as shown in Fig. 3. A longpass optical filter (T > 90% at 1114–2150 nm and R > 99.99% at 1030 nm) was employed to separate the Raman laser and fundamental laser. The utilization of OC with low transmission ($T_{OC}$ = 2%) resulted in coating damage on the surfaces of $YVO_4$ and $Cr^{4+}$:YAG crystals when $P_{in}$ > 4 W. Therefore, the $P_{in}$ was limited to 3.9 W for avoiding coating damage with $T_{OC}$ = 2%. The lasing threshold of Raman laser was about 2 W, 2.2 W, 1.9 W and 2 W for $T_{OC}$ = 2%, 6%, 11% and 16%. The Raman laser average output power increases almost linearly with $P_{in}$ for different $T_{OC}$s. The slope efficiencies were approximately 2.9%, 4.1%, 4.4% and 3.4% for $T_{OC}$ = 2%, 6%, 11% and 16%, respectively. The maximum Raman laser average output power of 53 mW was achieved at $P_{in}$ = 3.9 W for $T_{OC}$ = 2% with a corresponding optical-to-optical efficiency of 1.4%. For $T_{OC}$ = 6%, 11% and 16%, the maximum Raman laser average output power was 112 mW, 142.8 mW and 118.8 mW at $P_{in}$ = 5.25 W, respectively. And the corresponding optical-to-optical efficiency was 2.1%, 2.7% and 2.3%, respectively. The best performance was achieved with $T_{OC}$ = 11%.

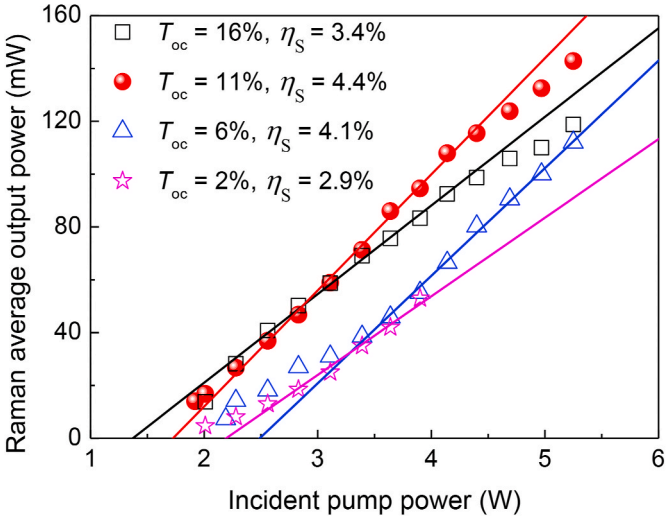


**Fig. 3.** Raman laser average output power of Yb:YAG/$Cr^{4+}$:YAG/$YVO_4$ PQSRML for $T_{OC}$ = 2%, 6%, 11%, 16% OC with $T_0$ = 90% $Cr^{4+}$:YAG versus $P_{in}$.

As shown in Fig. 3, the Raman laser average output power tended to increase slowly when $P_{in}$ exceeded 4.3 W for $T_{OC}$ = 11% and 16%. According to $P_{heat} = P_{S1}(\lambda_{S1}/\lambda_L\text{-}1)$ ($P_{S1}$ is the time-averaged power of first-order Stokes laser, and $\lambda_L$ and $\lambda_{S1}$ are the fundamental and first-order Stokes laser wavelengths, respectively) [27], the thermal loading ($P_{heat}$) in the Raman medium by the SRS process depends on the Raman output power. The higher Raman output power for the case of $T_{OC}$ = 11% and 16% resulted in more severe thermal effect, which declined the growth rate of output power under high pump power.

Fig. 4 shows the repetition rate, pulse width, pulse energy and peak power for the Stokes laser obtained in the Yb:YAG/$Cr^{4+}$:YAG/$YVO_4$ PQSRML varying with $P_{in}$ for different $T_{OC}$ in the case of $T_0$ = 90% $Cr^{4+}$:YAG. The repetition rate increases nearly linearly with $P_{in}$ for different

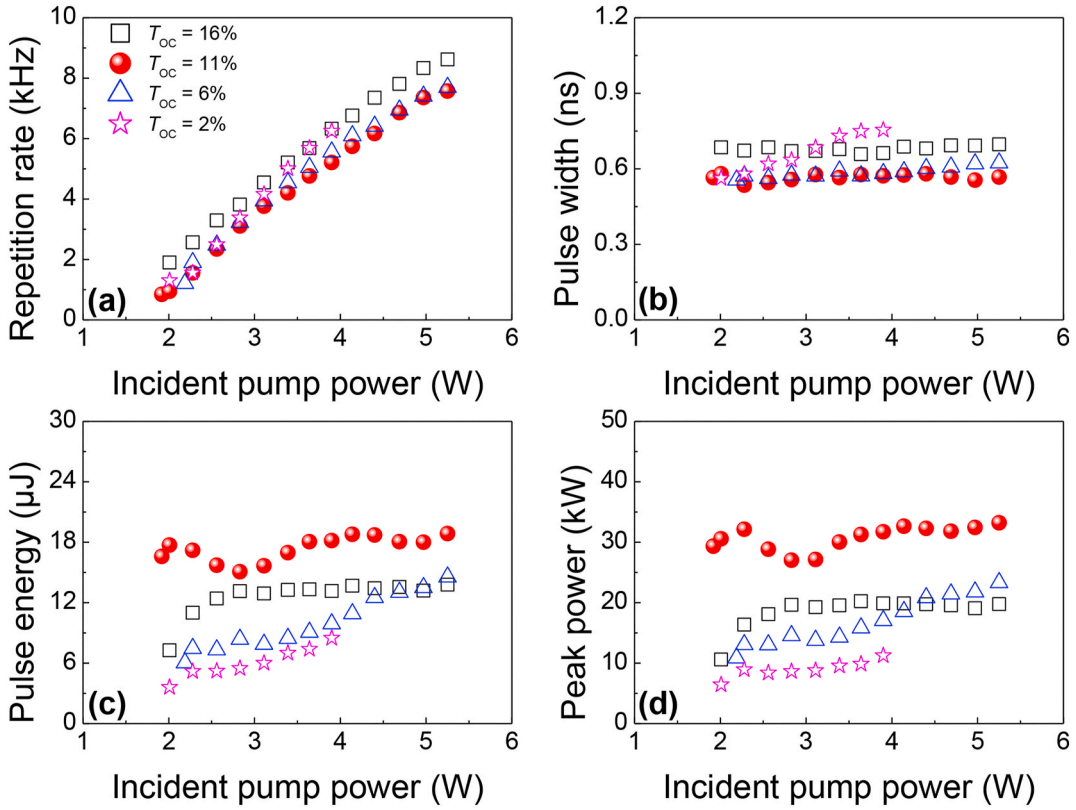


**Fig. 4.** (a) Repetition rate (R.R), (b) pulse width ($t_S$), (c) pulse energy ($E_S$) and (d) peak power ($P_{peak}$) for the Stokes laser of the Yb:YAG/$Cr^{4+}$:YAG/$YVO_4$ PQSRML versus $P_{in}$ for $T_{OC}$ = 2%, 6%, 11% and 16% with $T_0$ = 90% $Cr^{4+}$:YAG.

$T_{OC}$. While other pulse characteristics ($t_S$, $E_S$, $P_{peak}$) exhibits weak dependence on the pump power as $P_{in}$ is well above the SRS threshold. The optimal pulse performance (large pulse energy, high peak power and short pulse width) of Yb:YAG/$Cr^{4+}$:YAG/$YVO_4$ PQSRML was obtained with $T_{OC}$ = 11%. At $P_{in}$ = 5.25 W, the highest pulse energy and peak power reached 18.9 μJ and 33.2 kW, respectively. Meanwhile the corresponding repetition rate and pulse width were 7.57 kHz and 567 ps, respectively. The further increase of $T_{OC}$ from 11% to 16% shows a dramatic deterioration in the Raman pulse performance as shown in Fig. 4, which is attributed to the lower intracavity fundamental laser intensity induced by the low reflectivity of OC with $T_{OC}$ = 16%. The extraordinary increase of repetition rate for $T_{OC}$ = 16% may be caused by more thermal effect induced by the less efficient Raman laser performance of Yb:YAG/$Cr^{4+}$:YAG/$YVO_4$ PQSRML. The pump beam size decreases as the thermal effect becomes stronger with pump power increasing, which results in the pump power intensity increases [28]. Moreover, the initial transmission of $Cr^{4+}$:YAG may slightly increase with the temperature rising [29] due to the relative stronger thermal effect in the case of $T_{OC}$ = 16%. Therefore, the increase of repetition rate in Yb:YAG/$Cr^{4+}$:YAG/$YVO_4$ PQSRML for $T_{OC}$ = 16% occurs, as shown in Fig. 4(a). Table 1 summarizes output laser characteristics of Stokes laser at their corresponding available maximum pump power for different $T_{OC}$s.

**Table 1**
Output characteristics of the Yb:YAG/$Cr^{4+}$:YAG/$YVO_4$ PQSRML for various $T_{OC}$s[a].

| $T_{OC}$, % | $P_S$, mW | R.R, kHz | $E_S$, μJ | $P_{peak}$, kW | $t_S$, ps |
|---|---|---|---|---|---|
| 2 | 53 | 6.25 | 8.5 | 11.2 | 754 |
| 6 | 112 | 7.69 | 14.6 | 23.3 | 623 |
| 11 | 142.8 | 7.57 | 18.9 | 33.2 | 567 |
| 16 | 118.8 | 8.62 | 13.8 | 19.8 | 697 |

[a] $P_S$ – maximum average output power of Stokes laser, $E_s$ – maximum pulse energy of Stokes laser, $P_{peak}$ – maximum peak power of Stokes laser, $t_S$ – pulse width of Stokes laser.

Fig. 5 shows the typical pulse profiles and pulses trains in Yb:YAG/$Cr^{4+}$:YAG/$YVO_4$ PQSRMLs with $T_0$ = 90% $Cr^{4+}$:YAG for $T_{OC}$ = 2%, 6%, 11% and 16%. The pulse widths were recorded at their corresponding available maximum pump power for different $T_{OC}$s. Typical Raman pulse profiles with a sharp rising edge and a smooth falling edge were obtained. The pulse widths of 754 ps, 623 ps, 567 ps and 697 ps in full width at half maximum (FWHM) were obtained for $T_{OC}$ = 2%, 6%, 11% and 16%, respectively. The residual fundamental laser pulse widths were around 0.9–1 ns for different $T_{OC}$s. The pulse compression effect induced by SRS process results in a dramatic pulse shortening for Raman laser pulses compared with fundamental laser pulses. The pulse energies were 8.5 μJ, 14.6 μJ, 18.9 μJ and 13.8 μJ, therefore, the corresponding peak power were 11.2 kW, 23.3 kW, 33.2 kW and 19.8 kW for $T_{OC}$ = 2%, 6%, 11% and 16%, respectively. The results further confirm that compact resonator configuration of Yb:YAG/$Cr^{4+}$:YAG/$YVO_4$ PQSRML are favorable for achieving sub-nanosecond, high peak power Raman laser. Typical Raman pulse trains of Yb:YAG/$Cr^{4+}$:YAG/$YVO_4$ PQSRMLs with $T_{OC}$ = 2%, 6%, 11% and 16% at $P_{in}$ = 3.9 W are shown in Fig. 5(e)–(h). The repetition rates were measured to be 6.25 kHz, 5.56 kHz, 5.21 kHz and 6.33 kHz for $T_{OC}$ = 2%, 6%, 11% and 16%, respectively. Although the Raman laser oscillates in multi-longitudinal mode, the peak intensities fluctuation and pulse-to-pulse timing jitter are relatively small. The amplitude fluctuation of Raman laser pulse trains is calculated to be 1.72%, 2.54%, 1.78% and 2.33% for $T_{OC}$ = 2%, 6%, 11% and 16%, respectively. The time jitters were calculated to be 3.16%, 0.97%, 0.71% and 2.17%, respectively. Therefore, stable Raman laser pulse trains were achieved in the Yb:YAG/$Cr^{4+}$:YAG/$YVO_4$ PQSRMLs with $T_0$ = 90% $Cr^{4+}$:YAG.

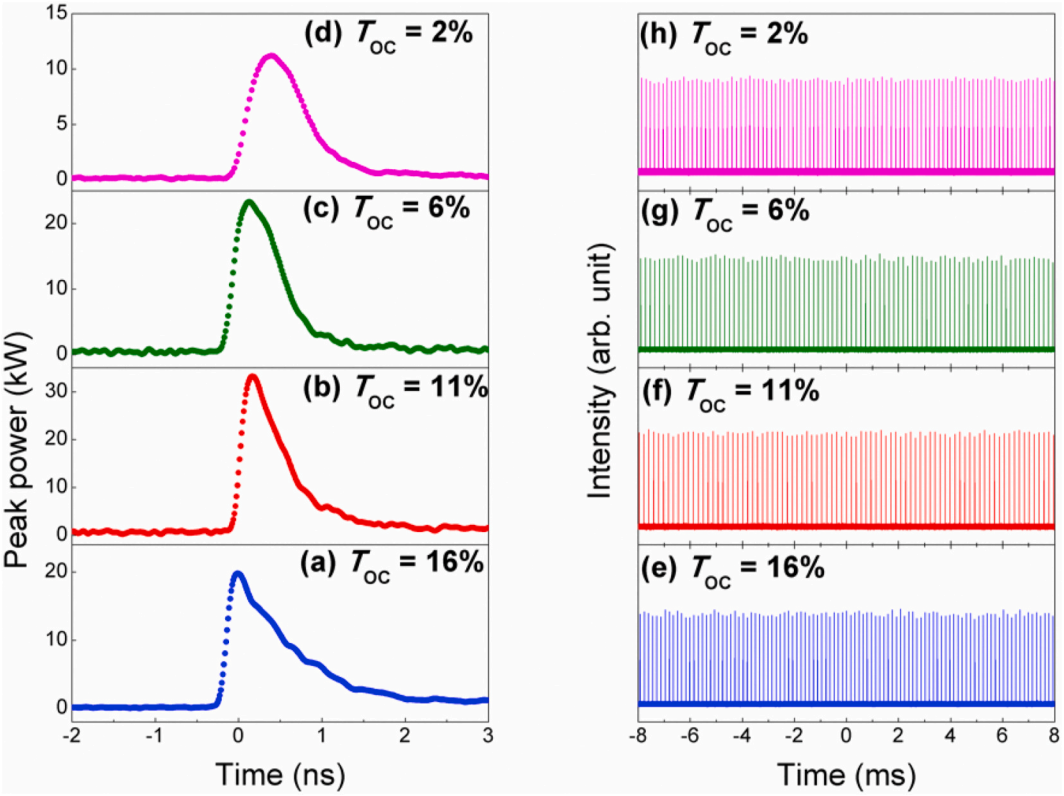


**Fig. 5.** (a)–(d) Typical pulse profiles and (e)–(h) pulse trains of Raman laser in the Yb:YAG/$Cr^{4+}$:YAG/$YVO_4$ PQSRML for different $T_{OC}$ with $T_0$ = 90% $Cr^{4+}$:YAG.

### 3.2. *Effects of $T_0$ on laser performance of Yb:YAG/$Cr^{4+}$:YAG/$YVO_4$ PQSRML*

The effects of $T_0$ on the performance of Yb:YAG/$Cr^{4+}$:YAG/$YVO_4$ PQSRML were carried out, and the output coupler with $T_{OC}$ = 16% was used. The typical lasing spectra of the Raman laser and fundamental laser with the combination of $T_0$ = 85% $Cr^{4+}$:YAG and $T_{OC}$ = 16% OC at different $P_{in}$ are shown in Fig. 6(a)-(c). The measured longitudinal modes separations for 1030 nm fundamental laser and 1134 nm Raman laser are approximately 0.70 and 0.83 nm, respectively, as shown in Fig. 6(a)–(c), which are about 14 times of the FSR of the Yb:YAG/$Cr^{4+}$:YAG/$YVO_4$ PQSRML determined by $\Delta\lambda = \lambda^2/2L_C$ [26]. The broad separations between adjacent longitudinal modes are attributed to the mode selection of combined etalon action introduced by 1.2 mm-thick Yb:YAG, 0.8 mm-thick $Cr^{4+}$:YAG, 3 mm-thick $YVO_4$ and 2 mm-thick OC. With further increase in $P_{in}$, spectral intensity of several longitudinal modes at short wavelength enhanced for both fundamental laser and Raman laser. The "blue shift" of emitting laser wavelength may be due to the asymmetric broad emission spectra of Yb:YAG crystal [28]. The intensifying competition among different longitudinal modes and the redistribution of the saturated inversion population under high pump power also impacted the emission spectra [30].

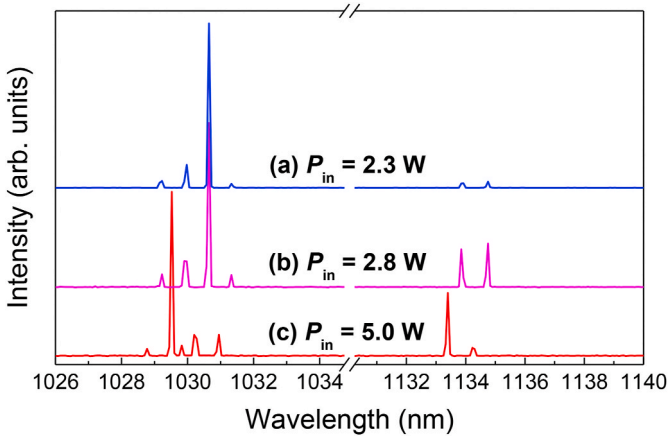


**Fig. 6.** Evolution of the laser emitting spectra of the Yb:YAG/$Cr^{4+}$:YAG/$YVO_4$ PQSRML with the combination of $T_0$ = 85% $Cr^{4+}$:YAG and $T_{OC}$ = 16% OC at different $P_{in}$.

The Raman laser average output power of Yb:YAG/$Cr^{4+}$:YAG/$YVO_4$ PQSRML for $T_0$ = 90% and 85% $Cr^{4+}$:YAG in the case of $T_{OC}$ = 16% is shown in Fig. 7. The lasing threshold of Raman laser with $T_0$ = 85% $Cr^{4+}$:YAG was measured to be approximately 2.28 W, which was slightly higher than that with $T_0$ = 90% due to the increased intracavity loss introduced by the lower $T_0$. For $T_0$ = 85% $Cr^{4+}$:YAG, the output power increases rapidly with $P_{in}$ and the slope efficiency is 5.5%, which is nearly 2 times of that for $T_0$ = 90% $Cr^{4+}$:YAG. There is no saturation tendency of Raman output power indicating that further scaling of output power was possible with increase in the pump power (see Fig. 7). The maximum Raman laser average output power reached 135 mW at $P_{in}$ = 5.25 W, and the corresponding optical-to-optical efficiency was 2.6%. Despite the output power and diode-to-Stokes laser efficiency (135 mW, 2.6%) is slightly lower compared to the results (142.8 mW, 2.7%) obtained with the combination of $T_{OC}$ = 11% OC and $T_0$ = 90% $Cr^{4+}$:YAG, the decrease in $T_0$ of $Cr^{4+}$:YAG is expected to realize the improvement of pulse performance.

The comparison of pulse performance on different $T_0$ of $Cr^{4+}$:YAG crystals with $T_{OC}$ = 16% is shown in Fig. 8. The superior pulse performance (shorter pulse width, higher pulse energy and peak power) was obtained with $T_0$ = 85% $Cr^{4+}$:YAG due to a larger modulation depth. For $T_0$ = 90% $Cr^{4+}$:YAG, the pulse energy and peak power exhibits slight independence on pump power at $P_{in}$ exceeding 2.5 W. While the pulse energy and peak power increases with $P_{in}$ and no obvious saturation tendency is observed for $T_0$ = 85%. The increasing tendency is mainly due to the incomplete bleaching under the available $P_{in}$ introduced by a

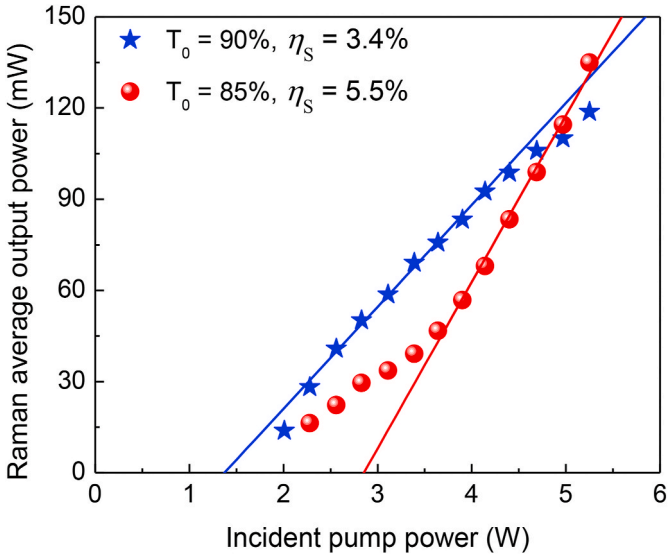


**Fig. 7.** Raman laser average output power of Yb:YAG/$Cr^{4+}$:YAG/$YVO_4$ PQSRML for $T_0$ = 85% and 90% $Cr^{4+}$:YAG with $T_{OC}$ = 16% versus $P_{in}$.

higher modulation depth of low $T_0$. The maximum pulse energy of 24.1 μJ with a pulse width of 535 ps at a repetition rate of 5.6 kHz was obtained at $P_{in}$ = 5.25 W. The corresponding maximum peak power was 45.1 kW. The experimental results reveal that the combination of $T_{OC}$ = 16% and $T_0$ = 85% $Cr^{4+}$:YAG exhibits better pulse performance as expected compared with the combination of $T_{OC}$ = 16% and $T_0$ = 90% $Cr^{4+}$:YAG. Table 2 summarizes output laser characteristics of Stokes laser with different $T_0$ of $Cr^{4+}$:YAG at $P_{in}$ = 5.25 W.

The narrowest pulse width of Raman laser was measured to be 505 ps while the fundamental laser pulse width was measured to be 920 ps at $P_{in}$ = 2.28 W, as shown in Fig. 9. Therefore, the pulse width of Raman laser was dramatically compressed compared to the residual fundamental laser.

## 4. Numerical simulation

The energy level diagram for a typical quasi-three-level Yb:YAG crystal is shown in Fig. 1(b). The $Yb^{3+}$ ions have only two manifolds, the upper state $^2F_{5/2}$ and lower state $^2F_{7/2}$. The temperature-dependent Boltzmann occupation factors can be used to describe the variation of the emission and absorption cross-sections of Yb:YAG crystal with temperature.

The modified coupled rate equations of passively Q-switched Raman micro-laser under CW LD pumping are established to describe the interaction of fundamental laser and Raman laser. By adding the SRS term and considering the quasi-three-level structure of $Yb^{3+}$ ions, the rate equations are given as follows [31–38]:

$$\frac{d\varphi_L}{dt}=\frac{l_g c\varphi_L}{l_c}\left(f_{21}^{l}\sigma_e^{l}N_2-f_{13}^{l}\sigma_{abs}^{l}N_1\right)-\frac{l_{Cr}c\varphi_L}{l_c}\left(\sigma_{gs}N_{gs}+\sigma_{es}N_{es}\right)-\frac{2g_{eff}h\nu_L c l_R\varphi_L\varphi_R}{t_r}-\frac{\varphi_L}{\tau_L}+k\frac{f_{21}^{l}N_2}{\tau} \quad (1)$$

$$\frac{d\varphi_R}{dt}=\frac{2\varphi_R}{t_r}\left(g_{eff}h\nu_L c\varphi_L l_R-\beta\sigma_g N_{gs}l_{Cr}-\beta\sigma_e N_{es}l_{Cr}\right)-\frac{\varphi_R}{\tau_R}+k_{SP}\varphi_L \quad (2)$$

**Table 2**
Output characteristics of the Yb:YAG/$Cr^{4+}$:YAG/$YVO_4$ PQSRML for different $T_0$.

| $T_0$, % | $P_S$, mW | R.R, kHz | $E_S$, μJ | $P_{peak}$, kW | $t_S$, ps |
|---|---|---|---|---|---|
| 85 | 135 | 5.6 | 24.1 | 45.1 | 535 |
| 90 | 118.8 | 8.62 | 13.8 | 19.8 | 697 |

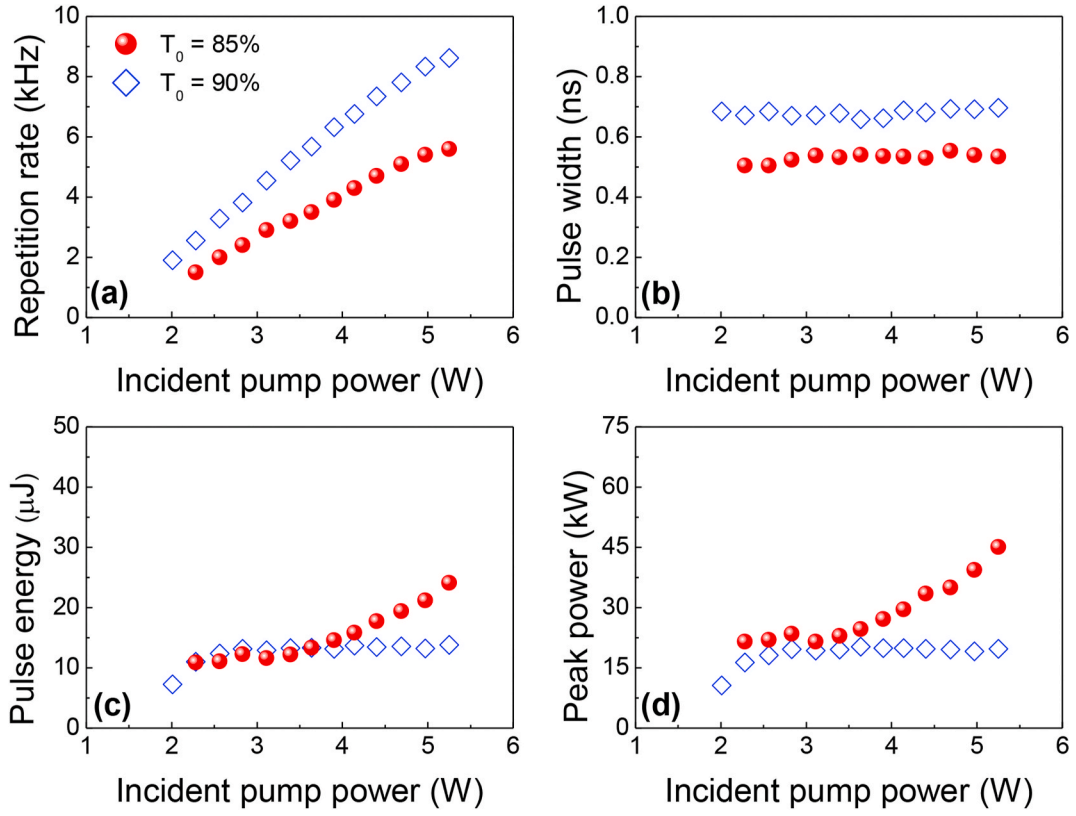


**Fig. 8.** (a) Repetition rate (R.R), (b) pulse width ($t_S$), (c) pulse energy ($E_S$) and (d) peak power ($P_{peak}$) for the Stokes laser of Yb:YAG/$Cr^{4+}$:YAG/$YVO_4$ PQSRML for $T_0$ = 85% and 90% $Cr^{4+}$:YAG with $T_{OC}$ = 16% OC versus $P_{in}$.

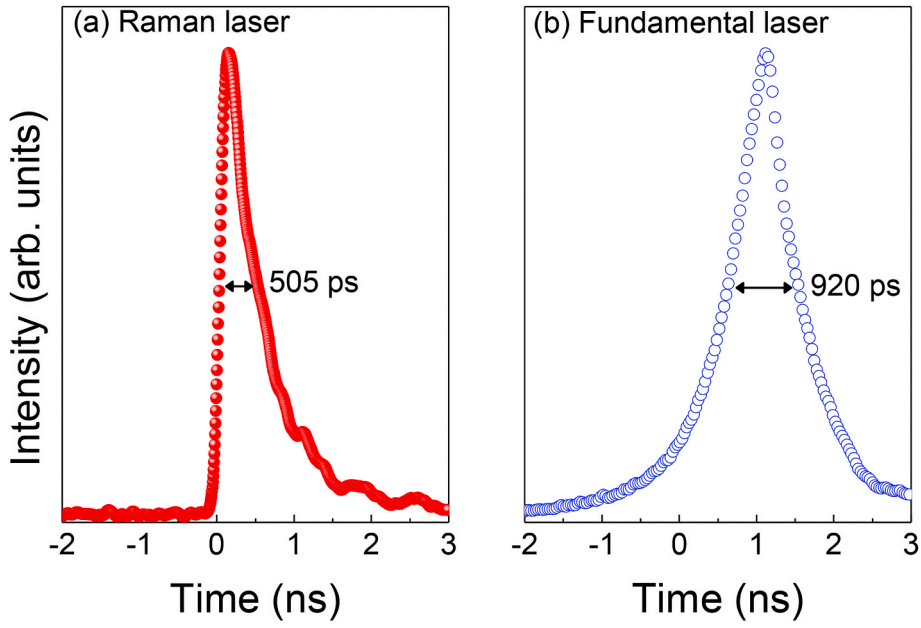


**Fig. 9.** Typical pulse profile of Raman laser and residual fundamental laser at $P_{in}$ = 2.28 W.

$$\frac{dN_1}{dt} = c\varphi_L\left(f_{21}^l\sigma_e^l N_2 - f_{13}^l\sigma_{abs}^l N_1\right) + \frac{N_2}{\tau} - W_p \tag{3}$$

$$\frac{dN_{gs}}{dt} = -\sigma_{gs}c\varphi_L N_{gs} - \beta\sigma_{gs}c\varphi_R N_{gs} + \frac{N_{s0} - N_{gs}}{\tau_s} \tag{4}$$

where $\varphi_L$ and $\varphi_R$ are the fundamental laser and Raman laser photon densities in the laser cavity, $N_1$ and $N_2$ are the lower ($^2F_{7/2}$) and upper ($^2F_{5/2}$) laser level population densities of the gain medium, $N_{gs}$ and $N_{es}$ are population densities at the ground state and excited-state of the $Cr^{4+}$:YAG crystal, respectively, $N_{total} = N_1 + N_2$ and $N_{s0} = N_{gs} + N_{es}$ are the total population densities of the laser gain medium and saturable absorber, respectively, $\sigma_e^l$ is spectroscopic emission cross-section ($\sigma_{\text{eff}}^l = f_{21}^l\ \sigma_e^l \approx 2.3 \times 10^{-20}$ cm$^{-2}$ at room temperature is usually defined as effective emission cross-section) [39], $\sigma_{\text{abs}}^l$ is the absorption cross-section at the fundamental laser wavelength of gain medium, $\sigma_{gs}$ and $\sigma_{es}$ are the absorption cross-sections of ground state and excited state of the $Cr^{4+}$:YAG at the fundamental laser wavelength, respectively, $\tau$ is the upper-level fluorescence lifetime of the laser gain medium, $\tau_s$ is the excited-state lifetime of the $Cr^{4+}$:YAG, $l_g$, $l_{Cr}$ and $l_R$ are the geometry lengths of laser gain medium, SA and Raman medium, $l_c$ is the optical length of cavity, $t_r = 2l_c/c$ is the cavity round-trip time, $c$ is the velocity of light in vacuum, $\tau_L = t_r/(\delta_l\text{-}lnR_l)$ and $\tau_R = t_r/(\delta_R\text{-}lnR_S)$ are the cavity lifetimes of fundamental laser and Raman laser photons, respectively, $\delta_l$ and $\delta_R$ are intracavity optical losses of fundamental laser and Raman laser, $R_l$ and $R_S$ are the reflectivity of the OCs for the fundamental laser and Raman laser, respectively, $k$ is the efficiency for the spontaneous photons contributing into the lasing mode, $h$ is the Planck constant, $\nu_L$ is the fundamental laser frequency, $\beta$ is the ratio of absorption cross-sections of saturable absorber at fundamental laser and Raman laser wavelengths, $K_{sp}$ is the spontaneous Raman scattering factor, and $W_p$ is the pump rate, which can be expressed as follows:

$$W_p = P_{in}\left\{1 - \exp\left[-\sigma_{abs}^p\left(f_{11}^p N_1 - f_{22}^p N_2\right)l_g\right]\right\} \Big/ \left(\pi\omega_p^2 h\nu_p l_g\right) \tag{5}$$

where $\omega_p$ is the average pump beam radius, $\sigma_{\text{abs}}^p$ is the absorption cross-section at pump wavelength of laser gain medium and $\nu_p$ is the frequency of the pump wavelength.

For quasi-three-level $Yb^{3+}$:YAG lasers, the re-absorption in the lower level has significant effect on the pulse performance and is described by the term "$f_{13}^l\ \sigma_{\text{abs}}^l N_1\varphi_L$". The thermal population distribution at terminated laser levels is strongly affected by the local temperature inside $Yb^{3+}$:YAG crystal. The theoretical estimation of the local temperature rising inside the Yb:YAG crystal ranged from 327 to 363 K for $P_{in}$ varying from 2.25 W to 5.25 W by applying the theoretical formula in Ref. [40]. The last term of Eq. (1) describes the spontaneous radiation contribution of cavity modes and the coefficient $k$ can be assumed as a relatively small value.

For intracavity Raman lasers, the actual effective Raman gain $g_{eff}$ of Raman crystals is lower than the ideal Raman gain coefficient considering the imperfect overlap in spatial and spectral profiles between fundamental laser and Raman laser modes [41,42]. Moreover, the spectral broadening of the fundamental laser modes induced by intracavity SRS process can further decrease effective Raman gain. Thus, the effective Raman gain $g_{eff}$ in the simulation modeling was estimated as 2.8 cm/GW, which indicated that a "Raman gain reduction factor" [42] value of approximately 0.62 with respect to the ideal Raman gain value of 4.5 cm/GW.

In order to analysis the relationship between the pulse characteristics with the transmissions of OCs theoretically and obtain the optimal transmission of OCs, the rate equations were solved numerically by the Runge–Kutta method. Parameters used for numerical simulation in the rate equations are listed in Table 3.

Two $Cr^{4+}$:YAG saturable absorbers with different $T_0$s ($T_0$ = 90%, 0.5 mm-thick and $T_0$ = 85%, 0.8 mm-thick) were used in the numerical simulation. Fig. 10 shows the dependence of Raman pulse energy and pulse width on $T_{OC}$s with two different $T_0$s. In the calculating process with $T_0$ = 85% $Cr^{4+}$:YAG, an extra added OC transmission of $T_{OC}$ = 18% (assuming the transmission of 20% for the Raman laser) was calculated to show completely a whole variation tendency of Raman pulse performance with further increase of $T_{OC}$. For the case of $T_0$ = 90% $Cr^{4+}$:YAG, $\delta_l$ and $\delta_R$ are assumed as 0.12 and 0.06, respectively. For the case of $T_0$ = 85% $Cr^{4+}$:YAG, $\delta_l$ and $\delta_R$ are assumed as 0.16 and 0.10, respectively. As indicated in Fig. 10(a), the optimum OC transmission ($T_{\text{OC-opt}}$) in terms of maximizing the Raman pulse energy increases with the decrease of $T_0$. The $T_{\text{OC-opt}}$ is close to 16% for $T_0$ = 85% $Cr^{4+}$:YAG, and 11% for $T_0$ = 90% $Cr^{4+}$:YAG. For a constant $T_0$, the pulse width is initially shortened steeply with the increase of $T_{OC}$ and then tends to change slowly with further increase of $T_{OC}$. The model indicates that a lower initial transmission of $Cr^{4+}$:YAG is desirable for scaling the Raman

**Table 3**
Spectroscopic and cavity parameters used for simulation modeling.

| Param. | Value | Ref. | Param. | Value | Ref. | Param. | Value | Ref. |
|---|---|---|---|---|---|---|---|---|
| $\sigma_e^l$ | $3.3 \times 10^{-20}$ cm$^2$ | [39] | $\sigma_{abs}^p$ | $0.76 \times 10^{-20}$ cm$^2$ | [39] | $\sigma_{es}$ | $8.2 \times 10^{-19}$ cm$^2$ | [35,43] |
| $\sigma_{abs}^l$ | $0.1 \times 10^{-20}$ cm$^2$ | [44] | $\sigma_{gs}$ | $4.6 \times 10^{-18}$ cm$^2$ | [35,43] | $N_g$ | $13.8 \times 10^{20}$ cm$^{-3}$ | [45] |
| $T$ | 951 μs | [39] | $\beta$ | 0.38 | [46] | $\omega_p$ | 90 μm | |
| $\tau_s$ | 3.4 μs | [35,43] | $K_{sp}$ | $2 \times 10^{-10}$ s$^{-1}$ | [36] | $\omega_R$ | 82 μm | |

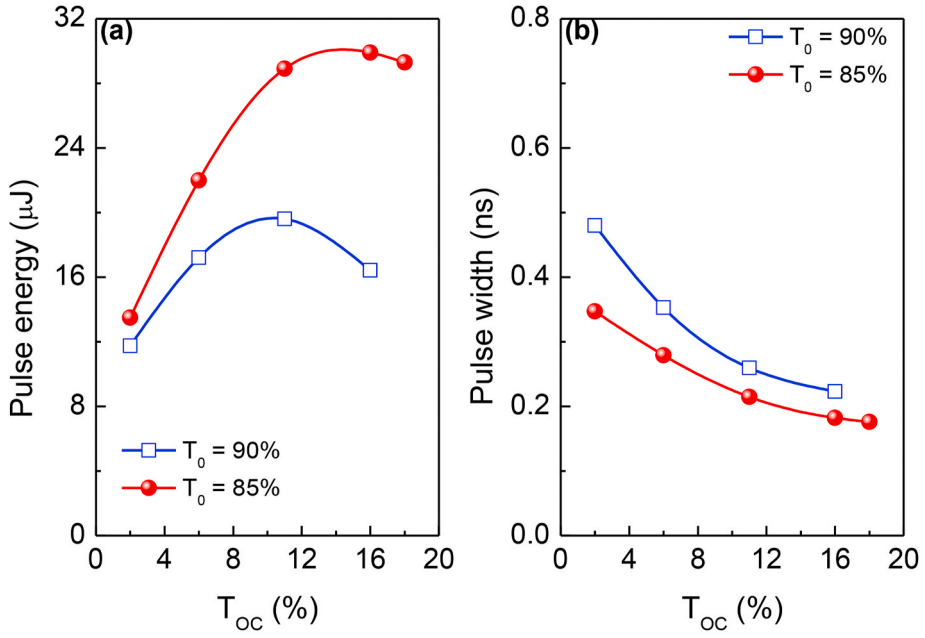


**Fig. 10.** (a) Pulse energy and (b) pulse width from Yb:YAG/$Cr^{4+}$:YAG/$YVO_4$ PQSRML as a function of $T_{OC}$ with $T_0 = 85\%$ and 90% $Cr^{4+}$:YAG at $P_{in} = 3.9$ W. The symbols represent the simulation values according to Eqs. (1)–(4). The solid curves are used to illustrate the variation tendency fitting to the simulation data.

pulse energy and shortening the pulse width when the $T_{OC}$ is set constant. Based on the numerical simulation model, it indicates that the utilization of $T_{OC} = 11\%$ and $T_{OC} = 16\%$ is close to optimum for the present micro-laser with $T_0 = 90\%$ $Cr^{4+}$:YAG and $T_0 = 85\%$ $Cr^{4+}$:YAG, respectively.

According to the general passively Q-switched laser model [32–35], the pulse energy and peak power are determined by the $T_0$ of $Cr^{4+}$:YAG and $T_{OC}$. For the present sandwich-type micro-laser configuration, it is reasonable to decrease $T_0$ for facilitating better pulse performance. Despite high intracavity fundamental laser intensity is more favorable for Raman conversion, the choice of $T_{OC}$ is limited by the re-absorption of $Yb^{3+}$ ions and the coating damage threshold of optical elements. In the experiment, coating damage on the surfaces of $YVO_4$ crystals, $Cr^{4+}$:YAG crystals and OCs occurred by the excessive intracavity intensity with the $T_{OC}$ less than 10% when $T_0 < 85\%$ $Cr^{4+}$:YAG crystal were used under high pump power levels. Consequently, an optimum combination of $T_0 = 85\%$ $Cr^{4+}$:YAG and $T_{OC} = 16\%$ OC was selected to enhance the Raman pulse performance by providing a large modulation depth and simultaneously avoiding unwanted coating damage.

A comparative study between the numerical simulation results and experimental results was performed at $P_{in} = 3.9$ W according to Eqs. (1)–(4). The dependence of Raman pulse characteristics on $T_{OC}$ is shown in Fig. 11. The pulse energy increases with the increase of $T_{OC}$ until the $T_{OC}$ approximately equals 11% and then decrease with further increase of $T_{OC}$. The FWHM pulse width of Stokes laser decreases sharply with $T_{OC}$ increase from 2% to 6%, and then tend to reduce slightly with continuous increase of $T_{OC}$. The broadening of pulse width at $T_{OC} = 16\%$ indicating a sudden deviation between the experimental result and its variation tendency curve may be due to the more thermal loading caused by less efficient SRS conversion process. And therefore the initial transmission of $Cr^{4+}$:YAG crystal may slightly increase with the temperature rising, which also leads to a slight increase of repetition rate as shown in Fig. 4(a). The variation of peak power and average output power versus $T_{OC}$ shows an analogous tendency with pulse energy. The optimal $T_{OC}$ for the best performance of peak power and average output power is close to $T_{OC} = 11\%$. The variation tendency of theory results is in fairly good agreement with that of experimental ones.

The deviations between numerical simulation values and experimental values are mainly attributed to the thermal effects. The above numerical model is a plane-wave approximation; therefore both the photon density and the inversion density distribution are assumed to be uniform, which is also result in the difference between the numerical simulation values and experimental values. Based on the numerical simulation model, it indicates that the utilization of $T_{OC} = 11\%$ is close to optimum for the present micro-laser with $T_0 = 90\%$ $Cr^{4+}$:YAG. For the design goal of passively Q-switched Raman lasers, the high peak power of Raman laser is significant. In general, the above theoretical numerical model can provide theoretical guidance for further optimization of LD pumped PQSRML.

## 5. Discussion

Table 4 summarizes output laser characteristics of this work and some analogous typical miniature passively Q-switched Raman lasers emitting around 1.1 μm. Compared with the previous works based on $Yb^{3+}$ ions doped laser gain medium, the results obtained in this work with the combination of $T_0 = 85\%$ $Cr^{4+}$:YAG and $T_{OC} = 16\%$ OC are superior in terms of Raman pulse width (505 ps, $P_{in} = 2.28$ W) and peak

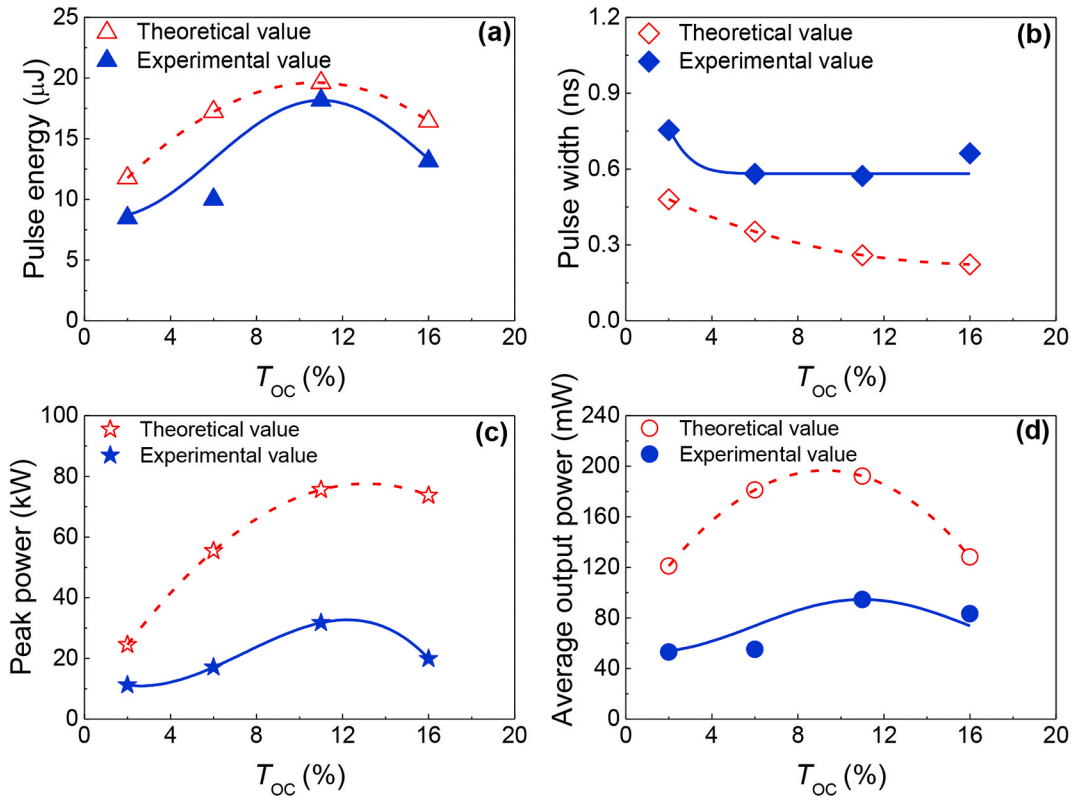


**Fig. 11.** Raman laser characteristics such as (a) pulse energy, (b) pulse width, (c) peak power and (d) average output power from Yb:YAG/$Cr^{4+}$:YAG/$YVO_4$ PQSRML as a function of $T_{OC}$ at $P_{in}$ = 3.9 W with $T_0$ = 90% $Cr^{4+}$:YAG. The solid and open symbols represent the experimental and numerical simulation values, respectively. The solid and dashed curves are used to illustrate the variation tendency of the Raman laser performance fitting to the experimental and simulation data, respectively.

**Table 4**
Summary of output parameters of $Cr^{4+}$:YAG passively Q-switched miniature Raman lasers[b].

| Crystal | $\lambda_S$, nm | $P_S$, mW | $E_S$, μJ | $P_{peak}$, kW | $t_S$, ns | Ref. |
|---|---|---|---|---|---|---|
| Yb:YAG/$YVO_4$ | 1134 | 135 | 24.1 | 45.1 | 0.505 | This work |
| Yb:YAG/$YVO_4$ | 1079–1260 | 82 | 4.04 | 9.2 | 0.44 | [20] |
| Yb:KLuW | 1151 | 119 | 3 | 1.5 | 2 | [18] |
| Yb:KLuW | 1139.3 | 1150 | 51 | 22.2 | 2.3 | [17] |
| Yb:KGW | 1145 | 110 | 8.2 | 11 | 0.7 | [14] |
| Yb:KGW | 1139 | 7 | 0.4 | 0.02 | 20 | [13] |
| Nd:$GdVO_4$/$YVO_4$ | 1164.4, 1174.7 | 104 | 0.83 | 1 | 0.825 | [8] |
| Nd:LSB/Ba$(NO_3)_2$ | 1196 | ~40 | 1.67 | 12.2 | 0.137 | [47] |
| Nd:LSB/Ba$(NO_3)_2$ | 1196 | ~90 | 1.2 | 5.7 | 0.118 | [37] |

[b] $\lambda_S$ –Stokes laser emission wavelength, $E_s$ – maximum pulse energy of Stokes laser, $P_{peak}$ – maximum peak power of Stokes laser, $t_S$ – shortest pulse width of Stokes laser.

power (45.1 kW, $P_{in}$ = 5.25 W). Remarkable shortening of the Raman pulse width is mainly attributed to the micro-laser setup of significantly reduced cavity length. The utilization of discrete laser gain medium and Raman medium configuration can provide good thermal management to avoid severe thermal loading, which is favorable for high peak power Raman laser generation.

The peak power of 45.1 kW obtained in this work is the highest value for stable Raman laser from the $Cr^{4+}$:YAG PQSRMLs under CW LD pumping condition to the best of our knowledge. A. A. Demidovich et al. has achieved 48 ps of Raman laser pulse width and corresponding 48 kW of Raman laser peak power at 1196 nm with $T_0$ = 78% $Cr^{4+}$:YAG from Nd:LSB/$Cr^{4+}$:YAG/Ba$(NO_3)_2$ PQSRML, unfortunate coating damage of crystals occurred under high peak power levels [47]. Therefore, the laser was unable to keep stable operation. While the Yb:YAG crystal has merits of long fluorescence lifetime (951 μs), low thermal loading (91% of quantum efficiency when pumped at 940 nm) and the capability of high concentration doping without remarkable reduction of laser performance. Therefore, the Yb:YAG crystal is more suitable as laser gain media for $Cr^{4+}$:YAG PQSRMLs and can keep stable operation at high peak power levels compared with the Nd:YAG crystal.

The output Raman laser beam profiles were monitored and measured at different absorbed pump powers. Although degradation of the beam quality introduced by thermal effects is inevitable, the Raman spatial beam profiles are nearly $TEM_{00}$ mode and the beam quality factor $M^2$ is less than 1.3 during the whole pumping region. Therefore, the thermal effect is not strong enough to affect the beam quality due to the property of Yb:YAG crystal and the low pump power level in the experiment. The aperture guiding effect has been demonstrated to benefit for the formation of cavity modes with good beam quality in end-pumped Yb:YAG lasers [48]. Moreover, in intracavity Raman lasers, the Raman beam clean-up effect also alleviates the beam degradation, which makes the Stokes laser beam tends to operate with better beam quality than the fundamental laser [27]. The utilization of discrete laser gain medium and Raman medium also provides good thermal management to avoid severe thermal loading. The polarization states of the Raman laser at different absorbed pump powers were checked by passaging the Raman laser through a linear polarizer. The elliptical polarization with different ellipticities was observed for Raman laser obtained in the Yb:YAG/$Cr^{4+}$:YAG/$YVO_4$ PQSRML.

Note that the present output couplers are common commercial products for 1 μm and the coating parameters are not specially designed for Raman laser wavelength. Moreover, the high-reflection coating of the rear surface of Yb:YAG crystal was originally designed for the

operation of 1.03 μm fundamental laser, and cannot cover entire 1030–1200 nm region leading to part of backward-propagating Raman laser leaked. Further promotion of Raman laser performance could be achieved by optimizing the coating parameters. For example, the HR region of the rear surface of Yb:YAG crystal should be extended to cover the Raman laser oscillation wavelength.

## 6. Conclusions

In conclusion, a sub-nanosecond, high peak power Yb:YAG/$Cr^{4+}$:YAG/$YVO_4$ PQSRML operating at 1134 nm Raman laser has been demonstrated. The maximum average output power of Raman laser was 142.8 mW with the combination of $T_{OC} = 11\%$ and $T_0 = 90\%$ $Cr^{4+}$:YAG. Enhanced Raman laser pulse performance of 24.1 μJ pulse energy and 45.1 kW peak power with a corresponding pulse width of 535 ps at a repetition rate of 5.6 kHz has been achieved by using a combination of $T_{OC} = 16\%$ and $T_0 = 85\%$ $Cr^{4+}$:YAG at $P_{in} = 5.25$ W. The shortest Raman pulse width of 505 ps was achieved at $P_{in} = 2.56$ W. The sandwich-type Yb:YAG/$Cr^{4+}$:YAG/$YVO_4$ PQSRML is an convenient and low-cost configuration for generating short pulses in several hundred-picosecond and pulse energy in several tens of micro-joule. The Yb:YAG/$Cr^{4+}$:YAG/$YVO_4$ PQSRML shows remarkable stability of the pulse trains. The sub-nanosecond, high peak power Yb:YAG/$Cr^{4+}$:YAG/$YVO_4$ PQSRML with commercial BK7 plane OCs provides a new method for developing miniature, low-cost Raman laser sources.

## Author statement

Manuscript title: Sub-nanosecond, high peak power Yb:YAG/$Cr^{4+}$:YAG/$YVO_4$ passively Q-switched Raman micro-laser operating at 1134 nm.

I have made substantial contributions to the conception or design of the work. Xiaolei Wang and Xiaojie Wang performed laser experiments and data analysis. Xiaolei Wang developed theoretical modeling and analysis; and they performed analysis, interpretation of the data for the work. Xiaolei Wang wrote the manuscript draft. I have revised it critically for important intellectual content; and I have approved the final version to be published. I agree to the accountable for all aspects of the work in ensuring that questions related to the accuracy of integrity of any part of the work are appropriately investigated and resolved. All authors read and contributed to the manuscript.

## Declaration of competing interest

The authors declare that they have no known competing financial interests or personal relationships that could have appeared to influence the work reported in this paper.

## Acknowledgments

This work was supported by National Natural Science Foundation of China (61475130, 61275143); Program for New Century Excellent Talents in University (NCET-09-0669).

## References

[1] R.P. Mildren, M. Convery, H.M. Pask, J.A. Piper, T. McKay, Efficient, all-solid-state, Raman laser in the yellow, orange and red, Optic Express 12 (5) (2004) 785–790.
[2] A.J. Lee, H.M. Pask, J.A. Piper, H.J. Zhang, J.Y. Wang, An intracavity, frequency-doubled $BaWO_4$ Raman laser generating multi-watt continuous-wave, yellow emission, Optic Express 18 (6) (2010) 5984–5992.
[3] T.S. Hawley, W.G. Telford, A. Ramezani, R.G. Hawley, Four-color flow cytometric detection of retrovirally expressed red, yellow, green, and cyan fluorescent proteins, Biotechniques 30 (5) (2001) 1028–1034.
[4] B.J. Bevis, B.S. Glick, Rapidly maturing variants of the Discosoma red fluorescent protein (DsRed), Nat. Biotechnol. 20 (1) (2002) 83–87.
[5] W. Telford, M. Murga, T. Hawley, R. Hawley, B. Packard, A. Komoriya, F. Haas, C. Hubert, DPSS yellow-green 561-nm lasers for improved fluorochrome detection by flow cytometry, Cytometry 68A (1) (2005) 36–44.
[6] W.G. Telford, S.A. Babin, S.V. Khorev, S.H. Rowe, Green fiber lasers: an alternative to traditional DPSS green lasers for flow cytometry, Cytometry 75A (12) (2009) 1031–1039.
[7] A.A. Kaminskii, K. Ueda, H.J. Eichler, Y. Kuwano, H. Kouta, S.N. Bagaev, T. H. Chyba, J.C. Barnes, G.M.A. Gad, T. Murai, J.R. Lu, Tetragonal vanadates $YVO_4$ and $GdVO_4$ - new efficient $\chi^{(3)}$-materials for Raman lasers, Optic Commun. 194 (1–3) (2001) 201–206.
[8] X.J. Wang, X.L. Wang, Z.F. Zheng, X.H. Qiao, J. Dong, 1164.4 nm and 1174.7 nm dual-wavelength Nd:$GdVO_4$/$Cr^{4+}$:YAG/$YVO_4$ passively Q-switched Raman microchip laser, Appl. Optic. 57 (12) (2018) 3198–3204.
[9] J. Dong, M. Bass, Y.L. Mao, P.Z. Deng, F.X. Gan, Dependence of the $Yb^{3+}$ emission cross section and lifetime on temperature and concentration in yttrium aluminum garnet, J. Opt. Soc. Am. B-Opt. Phys. 20 (9) (2003) 1975–1979.
[10] J. Dong, K.I. Ueda, A. Shirakawa, H. Yagi, T. Yanagitani, A.A. Kaminskii, Composite Yb:YAG/$Cr^{4+}$:YAG ceramics picosecond microchip lasers, Optic Express 15 (22) (2007) 14516–14523.
[11] X.Y. Guo, S. Tokita, J. Kawanaka, High beam quality and high peak power Yb:YAG/Cr:YAG microchip laser, Optic Express 27 (1) (2019) 45–54.
[12] P. Loiko, J.M. Serres, X. Mateos, K. Yumashev, A. Yasukevich, V. Petrov, U. Griebner, M. Aguilo, F. Diaz, Sub-nanosecond Yb:$KLu(WO_4)_2$ microchip laser, Opt. Lett. 41 (11) (2016) 2620–2623.
[13] A.A. Lagatsky, A. Abdolvand, N.V. Kuleshov, Passive Q switching and self-frequency Raman conversion in a diode-pumped Yb:$KGd(WO_4)_2$ laser, Opt. Lett. 25 (9) (2000) 616–618.
[14] V.E. Kisel, V.G. Shcherbitsky, N.V. Kuleshov, Efficient self-frequency Raman conversion in a passively Q-switched diode-pumped Yb:$KGd(WO_4)_2$ laser, in: Advanced Solid-State Photonics, Optical Society of America, 2003, pp. 189–192.
[15] A.S. Grabtchikov, A.N. Kuzmin, V.A. Lisinetskii, V.A. Orlovich, A.A. Demidovich, M.B. Danailov, H.J. Eichler, A. Bednarkiewicz, W. Strek, A.N. Titov, Laser operation and Raman self-frequency conversion in Yb:KYW microchip laser, Appl. Phys. B Laser Optic. 75 (6–7) (2002) 795–797.
[16] J.H. Liu, U. Griebner, V. Petrov, H.J. Zhang, J.X. Zhang, J.Y. Wang, Efficient continuous-wave and Q-switched operation of a diode-pumped Yb:$KLu(WO_4)_2$ laser with self-Raman conversion, Opt. Lett. 30 (18) (2005) 2427–2429.
[17] J.H. Liu, V. Petrov, H.J. Zhang, J.Y. Wang, Power scaling of a continuous-wave and passively Q-switched Yb:$KLu(WO_4)_2$ laser end-pumped by a high-power diode, Appl. Phys. B Laser Optic. 88 (4) (2007) 527–530.
[18] P. Loiko, J.M. Serres, X. Mateos, V. Jambunathan, K. Yumashev, V. Petrov, U. Griebner, M. Aguiló, F. Díaz, Passive Q-switching and self-Raman conversion in Yb:$KLu(WO_4)_2$ microchip laser, in: The European Conference on Lasers and Electro-Optics, Optical Society of America, 2015. CA_5b_3.
[19] V.E. Kisel, A.E. Troshin, N.A. Tolstik, V.G. Shcherbitsky, N.V. Kuleshov, V. N. Matrosov, T.A. Matrosova, M.I. Kupchenko, Q-switched $Yb^{3+}$:$YVO_4$ laser with Raman self-conversion, Appl. Phys. B Laser Optic. 80 (4–5) (2005) 471–473.
[20] X.L. Wang, X.J. Wang, J. Dong, Multiwavelength, sub-Nanosecond Yb:YAG/$Cr^{4+}$:YAG/$YVO_4$ passively Q-switched Raman microchip laser, IEEE J. Sel. Top. Quant. Electron. 24 (5) (2018) 8.
[21] O. Svelto, D.C. Hanna, Principles of Lasers, Springer, 2010.
[22] J. Liu, V. Petrov, H. Zhang, J. Wang, M. Jiang, Efficient passively Q-switched laser operation of Yb in the disordered $NaGd(WO_4)_2$ crystal host, Opt. Lett. 32 (12) (2007) 1728–1730.
[23] J.H. Liu, X.P. Tian, Z.C. Zhou, K. Wu, W.J. Han, H.J. Zhang, Efficient laser operation of Yb:$Lu_3Ga_5O_{12}$ garnet crystal, Opt. Lett. 37 (12) (2012) 2388–2390.
[24] J. Liu, X. Tian, K. Wu, Q. Dai, W. Han, H. Zhang, Highly efficient Q-switched laser operation of Yb:$Y_3Ga_5O_{12}$ garnet crystal, Optic Express 21 (3) (2013) 2624–2631.
[25] J. Liu, Q. Dai, Y. Wan, W. Han, X. Tian, The potential of Yb:$YCa_4O(BO_3)_3$ crystal in generating high-energy laser pulses, Optic Express 21 (8) (2013) 9365–9376.
[26] W. Koechner, Solid-state Laser Engineering, Spring-Verlag, Berlin, 1999.
[27] H.M. Pask, The design and operation of solid-state Raman lasers, Prog. Quant. Electron. 27 (1) (2003) 3–56.
[28] Y. Cheng, J. Dong, Y.Y. Ren, Enhanced performance of Cr,Yb:YAG microchip laser by bonding Yb:YAG crystal, Optic Express 20 (22) (2012) 24803–24812.
[29] M. Tsunekane, T. Taira, Temperature and polarization dependences of Cr:YAG transmission for passive Q-switching, in: Conference on Lasers and Electro-Optics/International Quantum Electronics Conference, Optical Society of America, Baltimore, Maryland, 2009, p. JTuD8.
[30] W.P. Risk, Modeling of longitudinally pumped solid-state lasers exhibiting reabsorption losses, J. Opt. Soc. Am. B-Opt. Phys. 5 (7) (1988) 1412–1423.
[31] V.V. Ter-Mikirtychev, M.A. Dubinskii, V.A. Fromzel, Q-switched, $TEM_{00}$-mode, diode-pumped $Yb^{3+}$:YAG laser with extended tunability, Optic Commun. 197 (4–6) (2001) 403–411.
[32] J. Dong, Numerical modeling of CW-pumped repetitively passively Q-switched Yb:YAG lasers with Cr:YAG as saturable absorber, Optic Commun. 226 (1–6) (2003) 337–344.
[33] Q. Li, B. Feng, D. Zhang, S. Du, Y. Shi, Z. Zhang, S. Zhang, Numerical solution and experiment of a self-Q-switched 946 nm Cr,Nd:YAG laser, Appl. Phys. B Laser Optic. 93 (2–3) (2008) 421–427.
[34] V.E. Kisel, A.S. Yasyukevich, N.V. Kondratyuk, N.V. Kuleshov, Diode-pumped passively Q-switched high-repetition-rate Yb microchip laser, Quant. Electron. 39 (11) (2009) 1018–1022.
[35] J. Ma, J. Dong, K. Ueda, A.A. Kaminskii, Optimization of Yb:YAG/$Cr^{4+}$:YAG composite ceramics passively Q-switched microchip lasers, Appl. Phys. B Laser Optic. 105 (4) (2011) 749–760.
[36] W.B. Chen, Y. Inagawa, T. Omatsu, M. Tateda, N. Takeuchi, Y. Usuki, Diode-pumped, self-stimulating, passively Q-switched $Nd^{3+}$:$PbWO_4$ Raman laser, Optic Commun. 194 (4–6) (2001) 401–407.

[37] A.A. Demidovich, P.A. Apanasevich, L.E. Batay, A.S. Grabtchikov, A.N. Kuzmin, V. A. Lisinetskii, V.A. Orlovich, O.V. Kuzmin, V.L. Hait, W. Kiefer, M.B. Danailov, Sub-nanosecond microchip laser with intracavity Raman conversion, Appl. Phys. B Laser Optic. 76 (5) (2003) 509–514.
[38] T.R. Schoepp, H.F. Tiedje, R. Fedosejevs, Characterisation and modelling of a passively Q-switched Yb:$CaF_2$ laser, IEEE J. Quant. Electron. 53 (6) (2017) 8.
[39] R.J. Beach, Optimization of quasi-three level end-pumped Q-switched lasers, IEEE J. Quant. Electron. 31 (9) (1995) 1606–1613.
[40] M.E. Innocenzi, H.T. Yura, C.L. Fincher, R.A. Fields, Thermal modeling of continuous-wave end-pumped solid-state lasers, Appl. Phys. Lett. 56 (19) (1990) 1831–1833.
[41] J.P. Lin, H.M. Pask, A.J. Lee, D.J. Spence, Study of relaxation oscillations in continuous-wave intracavity Raman lasers, Optic Express 18 (11) (2010) 11530–11536.
[42] D.C. Parrotta, A.J. Kemp, M.D. Dawson, J.E. Hastie, Multiwatt, continuous-wave, tunable diamond Raman laser with intracavity frequency-doubling to the visible region, IEEE J. Sel. Top. Quant. Electron. 19 (4) (2013) 8.
[43] Z. Burshtein, P. Blau, Y. Kalisky, Y. Shimony, M.R. Kokta, Excited-state absorption studies of $Cr^{4+}$ ions in several garnet host crystals, IEEE J. Quant. Electron. 34 (2) (1998) 292–299.
[44] L.D. Deloach, S.A. Payne, L.L. Chase, L.K. Smith, W.L. Kway, W.F. Krupke, Evaluation of absorption and emission properties of $Yb^{3+}$ doped crystals for laser applications, IEEE J. Quant. Electron. 29 (4) (1993) 1179–1191.
[45] T. Taira, W.M. Tulloch, R.L. Byer, Modeling of quasi-three-level lasers and operation of cw Yb:YAG lasers, Appl. Optic. 36 (9) (1997) 1867–1874.
[46] V.L. Kalashnikov, Pulse shortening in the passive Q-switched lasers with intracavity stimulated Raman scattering, Optic Commun. 218 (1–3) (2003) 147–153.
[47] A.A. Demidovich, S.V. Voitikov, L.E. Batay, A.S. Grabtchikov, M.B. Danailov, V. A. Lisinetskii, A.N. Kumin, V.A. Orlovich, Modeling and experimental investigation of short pulse Raman microchip laser, Optic Commun. 263 (1) (2006) 52–59.
[48] T.Y. Fan, Aperture guiding in quasi-three-level lasers, Opt. Lett. 19 (8) (1994) 554–556.